Available online at www.sciencedirect.com
ScienceDirect
Journal of Power Sources 159 (2006) 312–318
JOURNAL OF POWER SOURCES
www.elsevier.com/locate/jpowsour

Novel organic–inorganic poly (3,4-ethylenedioxythiophene) based nanohybrid materials for rechargeable lithium batteries and supercapacitors

A. Vadivel Murugan *

Centre for Materials for Electronics Technology (C-MET), Department of Information Technology, Government of India, Panchawati, Dr. Homi Bhabha Road, Pune 411008, India

Available online 30 May 2006

Abstract

Synthesis and characterization of poly (3,4-ethylenedioxythiophene) (PEDOT) interleaved between the layers of crystalline oxides of V and Mo is discussed with special emphasis on their application potential as electrodes for rechargeable Li batteries and supercapacitors. The expansion of the interlayer spacing of crystalline oxides (for example, V_2O_5 causes expansion from 0.43 to 1.41 nm) is consistent with a random layer stacking structure. These hybrid nanocomposites when coupled with a large-area Li foil electrode in 1 M $LiClO_4$ in a mixture of ethylene and dimethylcarbonate (1:1, v/v), give enhanced discharge capacity compared to pristine oxides. For example a discharge capacity of ~350 mAh g^{-1}, in the potential range 4.2–2.1 V (versus Li^+/Li) is obtained for PEDOT–V_2O_5 hybrid which is significantly large compared to that for simple Li-intercalated V_2O_5. The improvement of electrochemical performance compared with that of pristine oxides is attributed to higher electric conductivity, enhanced bi-dimensionality and increased structural disorder. Although these conducting polymer-oxide hybrids delivered more than 300 mAh g^{-1} in the potential range 1.3–4.3 V, their cycle life needs further improvements to realize their commercial potential. Similarly, the double layer capacitance of MoO_3 increases from ~40 mF g^{-1} to ~300 F g^{-1} after PEDOT incorporation in the interlayer gap of MoO_3 under similar experimental conditions and the nanocomposite displays intriguing effects with respect to electrochemical Li^+ insertion. The PEDOT–MoO_3 nanocomposite appears to be a promising electrode material for non-aqueous type supercapacitors.

Keywords: Advanced nanohybrid materials; Poly(3,4-ethlenedioxythiophene); V_2O_5; MoO_3; High capacity lithium batteries; Supercapacitor

1. Introduction

In recent years, electrochemical power sources such as rechargeable lithium-ion batteries and electrochemical capacitors have found many potential applications as power sources for electric vehicles, digital mobile telecommunication devices, pulsed light generators and medical instruments [1,2]. In addition, an exponential growth in portable electronics such as laptop computers and cellular phones has created enormous interest in the development of cheaper and environmentally benign lithium batteries. Thus research on development of eco-friendly and cost effective high capacity novel electrode materials for rechargeable lithium batteries and super capacitor is intense at present [2]. Recently, many new classes of nanocomposite electrode materials have been developed by insertion of the macromolecular species into two-dimensional layered transition metal oxides. In particular, conducting polymer based nanocomposites have received a considerable attention over past several years to integrate profitably many desirable properties of both transition metal oxide and the polymeric counterpart [1–8].

In this present study, we describe the electrochemical characterization of new organic–inorganic hybrids are prepared by intercalation of conducting poly (3,4-ethylenedioxythiophene) (PEDOT) into V_2O_5 and MoO_3 which has been used as a electrode materials for rechargeable lithium batteries and supercapacitor respectively. (i) PEDOT–V_2O_5 nanocomposite has been prepared by redox intercalation reaction of EDOT with crystalline V_2O_5 powder and the subsequent polymerization chemistry associated with this system to demonstrate the exis-

* Tel.: +91 20 25898390/141; fax: +91 20 25893044.
E-mail addresses: vadivel12@hotmail.com, vadivel1259@rediffmail.com.

0378-7753/$ – see front matter © 2006 Elsevier B.V. All rights reserved.
doi:10.1016/j.jpowsour.2006.04.033

tence of two phases in the PEDOT–V_2O_5 system corresponding to the intercalation of PEDOT into V_2O_5. These observations are supported by several physicochemical data and microstructure of PEDOT–V_2O_5 nanocomposites and the resulting nanocomposite shows improved room temperature conductivity and their outstanding electrochemical performance for high capacity cathode material for lithium batteries. (ii) In order to broaden the scope of these new hybrid electrode materials for electrochemical supercapacitors, we used molybdenum trioxide due to its inherent advantages compared to RuO_2 despite of its disadvantage including relatively slow kinetics for Li-ion transport, electronically insulating state upon full oxidation and poor cycling behavior [9]. One approach to modify the properties of a host material is through the intercalation of electronically conducting large guest species into the interlayer van der Waals gap, albeit with some difficulty. Resultant of these nanocomposites suggests that when these organo-inorganic hybrids are combined at "nanoscale" level, several new properties like enhanced electrochemical storage ability do emerge due to synergistic effects [10,11]. Here we report a new modification of the *in situ* intercalative polymerization reaction for the first time, which allows the intercalation of PEDOT nanoribbons into the van der Waals gap of MoO_3 to produce the nanocomposite. This nanocomposite is characterized by powder X-ray diffraction, X-ray photoelectron spectroscopy (XPS), scanning electron microscopy (SEM) and electronic conductivity measurements. Furthermore, the application potential of this nanocomposite, displaying some unusual interesting effects with respect to enhancement of electrochemical supercapacitor properties of MoO_3 by intercalation of PEDOT.

2. Experimental

2.1. Preparation of PEDOT–V_2O_5 nanocomposite

The mixtures of V_2O_5 (1.1 mM) and EDOT monomer (0.42 mM) in double distilled water were treated in double walled Teflon lined digestion vessel, placed on a turn-table for uniform heating using a microwave digestion system (MLS-120 Mega, GmbH, Germany). The outer shell of the reaction vessel was composed of a high strength polymer called Ultem polyetherimide, and the inner liner was composed of Teflon. These vessels were transparent to microwave and hence, the contents in these vessels could be heated hydrothermally. When, the reaction mixture was exposed to microwave radiation the microwaves induced rotation of the dipoles within the liquid, forcing the polar molecules to align and relax in the field of oscillating electromagnetic radiations causing the liquid to become hot. Thus the heat produced within the liquid is not transferred from the vessel as in other conventional systems. Computer-controlled microwave-hydrothermal treatments were conducted for different durations using 2.45 GHz microwave with full power (950 W) for 10 min. After the microwave irradiation, the solid was filtered off and washed repeatedly with water and ethanol and the dark bluish black powder was dried in air.

2.2. Exfoliation of Li_xMoO_3 and preparation of PEDOT–MoO_3 nanocomposite

The lithium molybdenum (Li_xMoO_3) bronze exfoliates readily in water to form a stable colloidal solution, and this indeed, makes it as an appealing candidate for the polymer intercalation. Thus 50 mg of lithium molybdenum bronze was exfoliated in 20 ml of double distilled water, and after 1 h sonication to form a suspension with a concentration of 5 g l^{-1}. To this suspension EDOT monomer (4.6 mM) was added drop wise and subsequently, 8.5 g of iron(III) chloride ($FeCl_3$) in 10 ml of water was added drop wise to the suspension as the oxidizing agent under microwave hydrothermal conditions for 10 min.

2.3. Characterization

Powder X-ray diffraction was carried out using Rigaku X-ray Diffractometer (Rigaku miniflex) equipped with a Ni filtered Cu Kα (1.542 Å) radiation and a graphite crystal monochromator. Electronic conductivity was measured on compacted pellets using a four probe conductivity method. X-ray photoemission spectra (XPS) were recorded on VG Microtech Multilab ESCA 3000 spectrometer using non-monochromatized Al Kα X-ray source ($h\nu = 1486.6$ eV). The base pressure in the chamber was maintained at 10^{-10} Torr range. The energy resolution of the spectrometer was set at 1.0 eV with Al Kα radiation at a pass energy of 50 eV. Binding energy (BE) calibration was performed with Au $4f_{7/2}$ core level at 83.9 eV and BE of adventitious carbon (284.9 eV) was utilized for charging correction with all the samples. The error in all the BE values reported here is within ±0.1 eV. Scanning electron microscopy (SEM) was carried out with Philips XL-30 microscope at an accelerating voltage of 20 kV after mounting samples on Al stubs with gold coatings. For TEM imaging (TEM model JEM-2010, JEOL) the powder was first dispersed in ethanol by ultrasonication, and then the suspension was drop casted on copper grid coated with carbon films and dried. The elemental analysis was carried out by inductive coupled plasma optical emission spectrometer (ICP-OES, Perkin-Elmer 1000) and CE-Instruments-EA 1110 CHNS-O Analyser. The electrochemical measurements were performed using a button-type cell configuration with the aid of a computer-controlled PGS201T (Tacussel) potentiostat/galvanostat system. The oxidized composite PEDOT–V_2O_5 cathodes were made by intimately mixing 70% (w/w) of the active material, 25% of Ketjenblack and 5% of PTFE. The surface area of electrodes and weight of the active material were adjusted to ∼1 cm^2 and ∼20 mg respectively for reproducibility. These electrodes were dried under vacuum at ∼80 °C for more than 3 h, and introduced into an argon-filled glove box without any exposure to air. The electrolyte was 1 M $LiClO_4$ in 1:1 mixture (v/v) of EC/DMC and a lithium foil was used as an anode. For charge/discharge experiments, a constant current of 15 mA g^{-1} was applied between 2.0 and 4.4 V (versus Li^+/Li). For cyclic voltammetry, the voltage was cycled between 2.2 and 3.8 V at a sweep rate of 0.5 mV s^{-1}. The electrochemical measurements were carried out by the crystalline MoO_3 and layered PEDOT–MoO_3 nanocomposite, at several scan rates illustrating supercapacitor behavior using 1 M

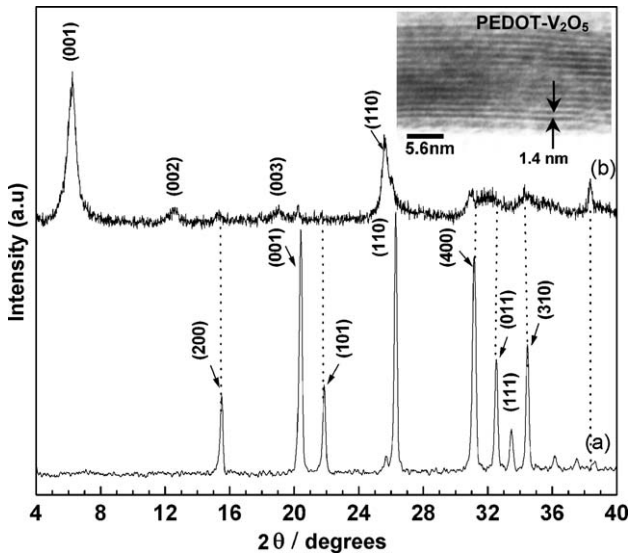

Fig. 1. Powder X-ray diffraction patterns of (a) pristine V_2O_5 and (b) PEDOT–V_2O_5 nanocomposite prepared by microwave irradiation. The inset figure shows the HRTEM image of PEDOT nanoribbons intercalated into V_2O_5 layers to form as a nanocomposite.

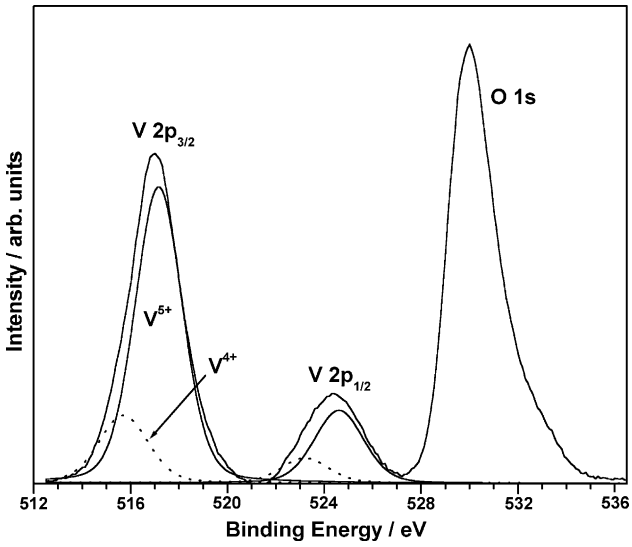

Fig. 2. X-ray photoelectron spectra of PEDOT–V_2O_5 nanocomposite prepared form redox intercalative polymerization.

$LiClO_4$ in EC/DMC (1:1, v/v) in between −1.5 and 0.25 V versus Ag/Ag^+ reference electrode.

3. Result and discussion

3.1. PEDOT–V_2O_5 nanocomposite

Fig. 1 shows a comparison of the powder XRD diffraction patterns of the (a) crystalline V_2O_5 and (b) PEDOT–V_2O_5 composite to demonstrate the subtle structural changes upon intercalation. The strongest peak observed at the low angle of corresponding to the (0 0 1) plane of the layered V_2O_5 structure is directly related to the interlayer spacing. The main features of the V_2O_5 diffraction pattern are in the composites are clearly modified by the appearance of a sharp diffuse scattering feature and the *d*-spacing increases from 4.3 to 14.1 Å. This would indicate that the expansion proceeds forming monolayer of polymer between V_2O_5 layers. It is noted that (*h k* 0) reflections of the hybrids correspond to those of the pristine V_2O_5 and that some of them, such as (1 1 0) and (3 1 0), show a diffuse peak shape, rising rather rapidly and then declining slowly toward high angle side. This feature suggests that the compounds have a random layer stacking structure, which consists of equidistant, and parallel (a–b) layers, but randomly rotated about the normal *c*-axis [11].

More significantly, high resolution transmission electron microscopy (HRTEM) image shows nanoribbon morphology of the PEDOT–V_2O_5 nanocomposite, as illustrated in Fig. 1 (inset), thus suggesting that the *in situ* redox intercalative polymerization is topotactic and the structure of the host still remain unchanged. As can be seen from HRTEM image, the V_2O_5 host consists of several conducting polymer nanoribbons and the low scattering power causes bright contrast for white lines, each about ∼1.4 nm between two dark fringes of vanadate layers. The same ribbon thickness of about 1.41 nm can be evaluated from the most pronounced intensity maximum found in the broad X-ray diffraction pattern *d*(0 0 1) (Fig. 1b). Thus, from the HRTEM image of the nanocomposite material, we conclude that the highly crystalline vanadium oxide is separated by alternating organic conducting polymer nanoribbons in this hybrid material.

X-ray photoelectron spectroscopy (XPS) is a surface specific technique to study the polymer–V_2O_5 interaction and vanadium (V^{5+}/V^{4+}) oxidation state, after the redox polymer intercalation. XPS results from V 2p and O 1s core level of polymer intercalated nanocomposite are displayed in Fig. 2. The spectra are presented after the removal of O 1 s X-ray satellite around 518–520 eV and after Shirley background subtraction. A low BE feature is apparent along with V^{5+} species at 517.2 eV. Deconvolution of the V 2p core levels clearly shows the above low BE feature at 515.7 eV, which is attributed to V^{4+}. The above BE values are in good correspondence with the standard compounds [12]. Using the deconvoluted peak area and the photoionization cross section of the V $2p_{3/2}$ level, the amount of V^{4+} is calculated to be 19% in total vanadium. This clearly indicates a charge transfer from polymer to V_2O_5 indicating the effectiveness of the interaction between polymer and V_2O_5. It is speculated here that the above interaction might be through S atom of polymer, as it is electron-rich; however the above suggestion could not be confirmed since the S 2p signal is hardly seen in XPS, perhaps due to low photoionisation cross section [13] and further work is in progress with different amount of polymer incorporation into V_2O_5.

The electrical transport behavior of nanocomposite can be understood by considering the insertion of PEDOT in V_2O_5 powder as a composite system in which, two different type of low-dimensional electronic conductors coexist at the molecular level in a dimensionally constrained environment. Two types of charge carriers can be present in these materials, small polarons (electrons) associated with the d^1 (V^{4+}) centers on the vanadium

Table 1
Comparison of interlayer spacing, composition analysis and electronic conductivity of PEDOT–V_2O_5 and PEDOT–MoO_3 nanocomposite and its counterparts

Sample	Interlayer spacing (Å)	Composition as per elemental analysis	Electronic conductivity at R.T., σ (S cm^{-1})
V_2O_5	4.34	V_2O_5	8.78×10^{-5}
PEDOT–V_2O_5	14.01	$(C_6H_4O_2S)_{0.026}V_2O_{4.9}$	2.92×10^{-3}
MoO_3	6.93	$MoO_{2.8}$	3.78×10^{-5}
Li_xMoO_3	8.27	$Li_{0.6}MoO_3$	1.3×10^{-2}
PEDOT–Li_xMoO_3	13.46	$Li_{0.3}(H_2O)_{0.48}(C_6H_4O_2S)_{0.35}MoO_3$	1.82×10^{-1}

oxide lattice, and large polarons on the PEDOT backbone. The actual nature of charge transport would depend on the relative mobility of these two different-kind of carriers as demonstrated by the fact that the electronic conductivity of PEDOT–V_2O_5 is 10^2 times higher than that of pristine V_2O_5. In all samples, the conductivity is almost exclusively electronic and increases with increase in the temperature as seen in most intercalated compounds and conjugated polymers [3–6] (see Table 1).

Fig. 3 demonstrates potential versus capacity curves of the first two cycles for the pristine V_2O_5 and nanocomposites. The pristine V_2O_5 shows distinctive plateaus due to structural changes [14], whereas the potential decreases more smoothly down to ~2.7 V for the hybrid samples. Similar continuous decrease in potential has been also observed for V_2O_5 xerogel [15], 2D-V_2O_5 [16] and conductive polymer–V_2O_5 xerogel nanocomposites [3–5], of which common structural feature is the separation of vanadium oxide layers owing to the presence of interlayer molecules. It would be, hence, a plausible explanation that the disturbed layer stacking derived by the separation of layers would make structural disorders, *e.g.* reduced covalency of bondings between some vanadium and oxygen atoms, which thereby creates empty sub-bandgap V^{5+}:$3d^0$ energy states rather uniformly distributed between ~3.7 and ~2.7 V [16]. The next lithium insertion into the pristine V_2O_5 occurs at ~2.3 V and is accompanied by the irreversible structural changes to γ-$Li_xV_2O_5$ phase [14], while the hybrids display a plateau at ~2.5 V like V_2O_5 xerogel or 2D-V_2O_5. It is worth to mention

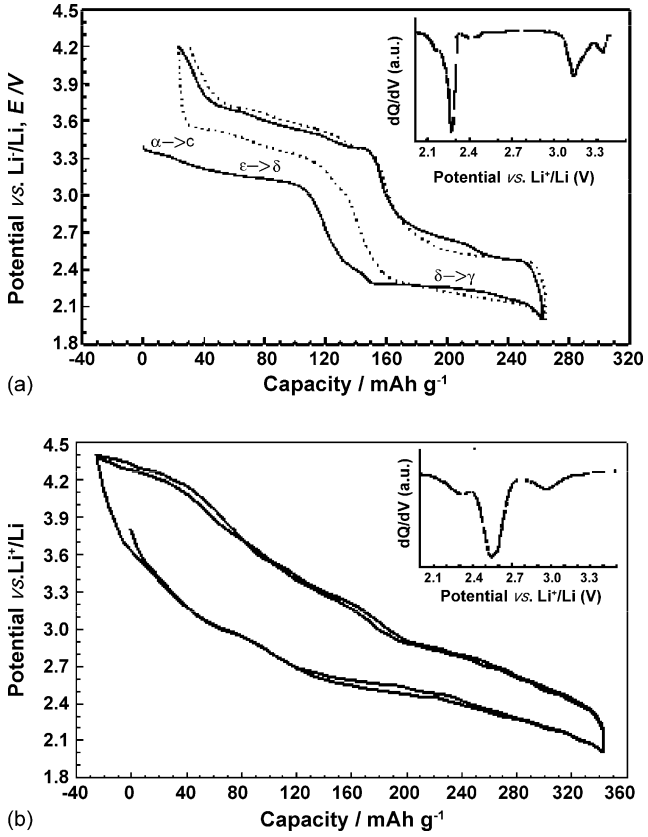

Fig. 3. Potential vs. capacity curves for the first two cycles of (a) pristine V_2O_5 and (b) PEDOT–V_2O_5 nanocomposite (insets show the corresponding differential capacity profiles of the first discharge). The potential range was set to 2.0–4.4 V vs. Li and current density was fixed to 15 mA g^{-1}.

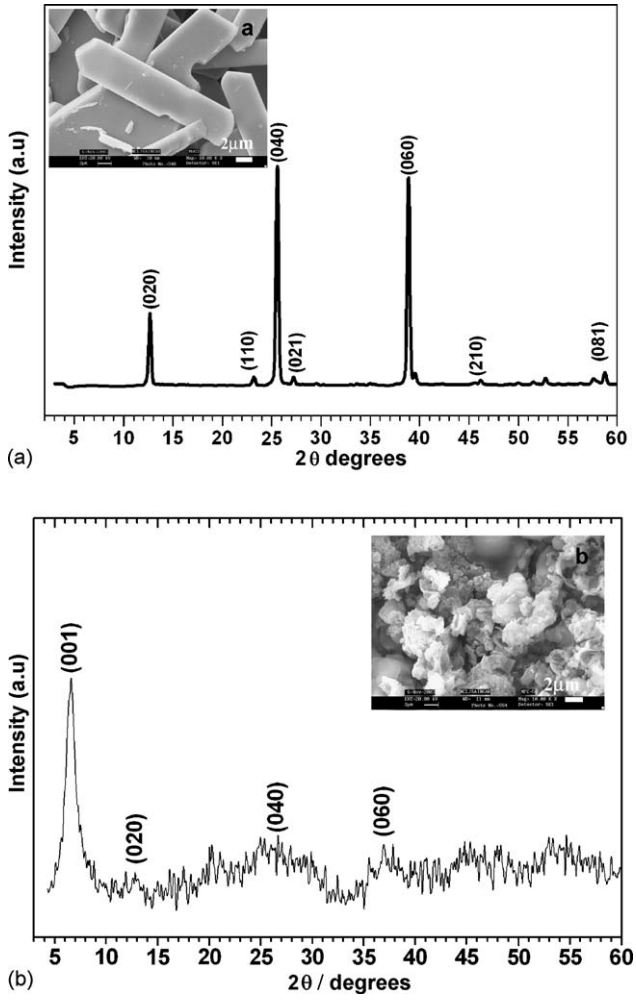

Fig. 4. A comparative powder X-ray diffraction patterns of (a) crystalline MoO_3 powder and (b) PEDOT–MoO_3 nanocomposite. The inset figures shows the SEM micrographs of corresponding (a) crystalline MoO_3 and (b) PEDOT–MoO_3 nanocomposites.

that the PEDOT–V_2O_5 nanocomposite reveals a larger capacity in the first charge process than in the first discharge. It would be accounted for the presence of V^{4+}, which can be easily oxidized by an electrochemical method, as already observed in the case of PPY–V_2O_5 and PTH–V_2O_5 nanocomposites [3–5]. It is noted that PEDOT–V_2O_5 nanocomposite shows the largest reversible capacity (∼330 mAh g^{-1}). The nanocomposites provide larger capacity than the pristine V_2O_5 and the improved performances are presumably due to a higher electrical conductivity and to the separation between vanadium oxide layers, leading to an enhanced bidimensionality.

3.2. PEDOT–MoO_3 nanocomposite

Fig. 4 shows a comparative X-ray diffraction pattern of (a) pristine MoO_3 and (b) polymer intercalated PEDOT–MoO_3 nanocomposite. However, increase in the interlayer distance of the pristine oxide, MoO_3, from $d = 6.93$ (0 2 0) to 13.46 Å (0 0 1), for PEDOT–MoO_3 composite indicates substantial incorporation of conducting polymeric material between the layers. In addition, the change in the interlayer distance is consistent with the interstitial PEDOT nanoribbons being oriented with the planes of the thiophene rings perpendicular to the layers as evident from the intense sharp peaks. Therefore, considerable bonding interaction between the organic and inorganic components is expected probably due to the hydrogen bonding.

A comparison of the SEM images of the MoO_3 and synthesized PEDOT–MoO_3 nanocomposite is presented in Fig. 4a and b (inset) respectively. It is apparent that PEDOT–MoO_3 composite forms a continuous and relatively homogeneous matrix with a lamellar morphology and that the incorporation of PEDOT into the MoO_3 accompanies morphological changes in agreement with the results of XRD patterns. This result also is in good agreement with a highly crystalline vanadium oxide separated by alternating organic conducting polymer nanoribbons in this organic–inorganic hybrid.

Since XPS is known to be very sensitive to the changes in electron density, it could be exploited well to study such changes in related systems [17]. XPS results for PEDOT and PEDOT–MoO_3 composites in terms of S 2p, C 1s and Mo 3d core levels are shown in Fig. 5a–c, respectively. More significantly, S 2p core level from PEDOT displays a peak at 164 eV, typical for thiophene sulfur [18]. However the S 2p core level binding energy (BE) from PEDOT–MoO_3 shows a peak around 165 eV suggesting charge transfer from sulfur atoms upon PEDOT intercalation. Carbon 1s core level also shows similar changes before and after the intercalation. In sharp contrast, PEDOT shows a single but broad C 1s peak at 285.3 eV, since the BE of carbon atoms from thiophene and ethylenedioxy groups are somewhat similar and hence are difficult to resolve. However upon intercalation, a broadening on the lower BE side and the appearance of a second peak are visible. The C 1s peak around 286 eV is attributed to ethylenedioxy group and the lower BE peak at 284 eV is attributed to the thiophene carbon atoms. The above shift in C 1s BE of thiphene group on intercalation suggests an increase in charge along with a broadening due to delocalization. In comparison, the ethylenedixoy groups remain at the same BE indicating that insignificant electronic involvement from this group. Mo $3d_{5/2}$ core level at 232.5 eV from PEDOT–MoO_3 composite is typical for MoO_3 [17] and the XPS studies hint oxidation of PEDOT after intercalation into MoO_3 along with some charge transfer from sulfur to MoO_3. Thus the XPS results are in good agreement with results from XRD and other characterization techniques. The room temperature conductivity for the PEDOT–MoO_3 composite is 1.82×10^{-1} S cm^{-1}, which is four order of magnitude higher compared to that of the pristine

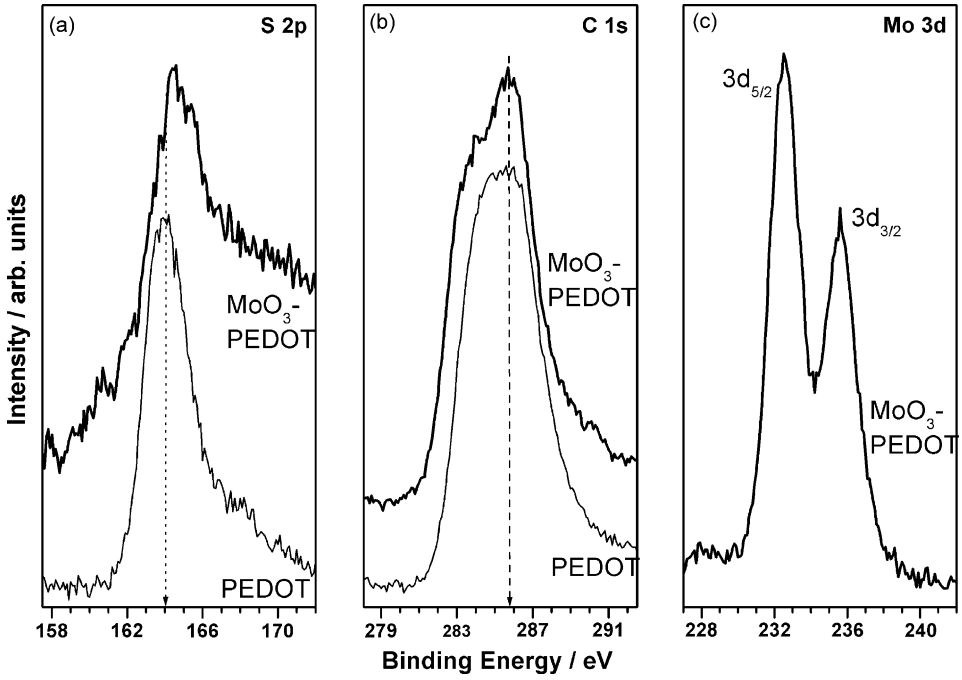

Fig. 5. X-ray photoelectron spectra from (a) S 2p, (b) C 1s and (c) Mo 3d core levels of PEDOT and PEDOT–MoO_3 nanocomposite.

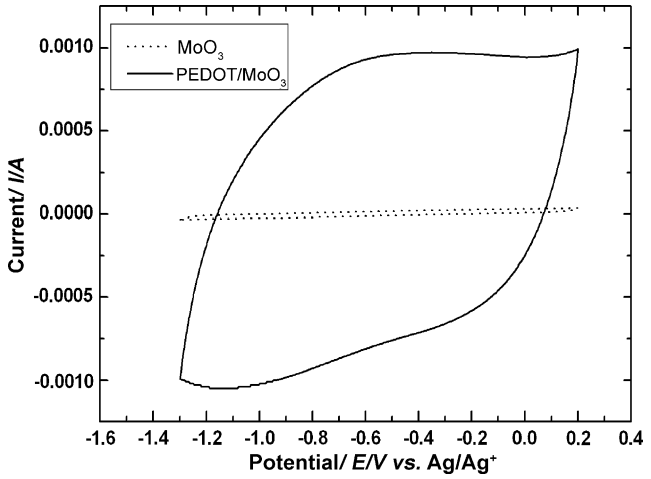

Fig. 6. Super imposed cyclic voltammograme of MoO_3 and PEDOT–MoO_3 nanocomposite at 300 mV s^{-1} illustrating the supercapacitor behavior using 1 M $LiClO_4$ in EC/DMC (1:1, v/v).

oxide, although pristine molybdenum trioxide is an insulator with a room temperature conductivity of 3.78×10^{-5} S cm^{-1} [19,20] (Table 1).

Super-imposed cyclic voltammograms of crystalline MoO_3 and PEDOT–MoO_3 nanocomposite at scan rate of 300 mV s^{-1} using 1 M $LiClO_4$ in EC/DMC (1:1, v/v) as the electrolyte is shown in Fig. 6, illustrating a drastic change in electrochemical properties induced by the polymer insertion. The observed linear current increase with scan rate is expected for a strongly adsorbed electrochemical species on the electrode surface. It is interesting to note that the electrochemical double layer capacitance of pristine MoO_3 increases from ~40 mF g^{-1} to ~300 F g^{-1} after polymer intercalated into MoO_3. During the first cathodic scan, *i.e.* when the voltage changes from −1.5 to 0.25 V versus Ag/Ag^+, the crystalline MoO_3 undergoes a well-known phase transformation and the stabilization of this becomes more prominent after the fourth cycle, suggesting that the structural change is permanent. Further, the weak interactions between the interlamellar layers, allow fast insertion of Li^+ ions between the ribbons rather than that in the crystalline molybdenum trioxide [19,20]. In contrast, for the PEDOT–MoO_3 hybrids, there is no sign of any irreversible structural change; however, the broad cathodic peak, resembles that of 2D inorganic layered compounds [11]. The broad and diffuse peak shape can, therefore, be correlated with the layer stacking derived by the polymer incorporation, as previously deduced from the X-ray diffraction.

4. Conclusion

The interlayer spacing of V_2O_5 expands by intercalation of PEDOT from 4.32 to 14.1 Å as detected from powder X-ray diffraction patterns, while X-ray photoelectron spectra show the presence of both V^{4+}/V^{5+} species in the nanocomposite also suggesting this reduced species V^{4+} in the V_2O_5 slabs due to oxidative polymerization. These results also do confirm the redox intercalation process and charge transfer from the polymer to the V_2O_5 framework. From the TEM results, it has been found that the incorporation of PEDOT nanoribbons increases bidimensionality of the V_2O_5 host by the layer separation. We observed that, the electrochemical measurements, of the nanocomposites showed reversible specific capacities up to ~330 mAh g^{-1} at 15 mA g^{-1}. This improvement of electrochemical performance compared with pristine V_2O_5 is attributed to higher electric conductivity and enhanced bidimensionality.

We have also employed a novel approach to prepare PEDOT–MoO_3 nanocomposite by using a soft chemistry route. This reaction takes place with the *in situ* oxidative polymerization in the presence of an external oxidizing agent. Our results suggest that the interlayer spacing, upon intercalation expands from 6.93 to 13.46 Å followed by exfoliation and restacking process. The resultant interlayer separation is consistent with the existence of two phases of organic and inorganic species in the nanocomposite corresponding to the intercalation of PEDOT in the MoO_3 framework to produce a new composite. Although, the relative conductivity is a linear function of PEDOT content, there is a four order of magnitude increase in conductivity compared to that of the pristine oxide afforded by the incorporation of the polymer. More importantly, the double layer capacitance of pristine MoO_3 increases from ~40 mF g^{-1} to ~300 F g^{-1} after PEDOT incorporation into MoO_3 under similar experimental conditions and the nanocomposite displays intriguing effects with respect to electrochemical Li^+ insertion. Thus PEDOT–MoO_3 nanocomposite appears to be a promising electrode material for non-aqueous type supercapacitors and this hybrid strategy pursued here provides an efficient way to fabricate cheap supercapacitor electrodes.

Acknowledgments

AVM would like to thank Ministry of Communication and Information Technology, Govt. of India, New Delhi and Executive Director, C-MET, Pune, India, to present this work in International Conference on Materials for Advanced Technology (ICMAT-2005), Singapore. I gratefully acknowledge to Dr. K. Vijayamohanan and Dr. Chinnakonda S. Gopinath, Scientists from NCL and Dr. Guy Campet, Dr. M.H. Delville, Research Directors, Dr. C.W. Kwon and M. Quintin from ICMCB, CNRS, France.

References

[1] B.E. Conway, J. Electrochem. Soc. 138 (1991) 1539.
[2] Y.U. Jeong, A. Manthiram, J. Electrochem. Soc. 148 (2001) A 189.
[3] M.G. Kanatzidis, C.G. Wu, J. Am. Chem. Soc. 111 (1989) 4141.
[4] M. Lira-Cantu, P. Gomez-Romero, J. Electrochem. Soc. 146 (1999) 2029.
[5] G.R. Goward, F. Leroux, L.F. Nazar, Electrochim. Acta 43 (1998) 1307.
[6] A. Vadivel Murugan, B.B. Kale, C.W. Kwon, G. Campet, K. Vijayamohanan, J. Mater. Chem. 11 (2001) 2470.
[7] A. Vadivel Murugan, C.W. Kwon, G. Campet, B.B. Kale, T. Maddanimath, K. Vijayamohanan, J. Power Sources 105 (2002) 1.
[8] C.W. Kwon, A. Vadivel Murugan, G. Campet, J. Portier, B.B. Kale, K. Vijaymohanan, J.-H. Choy, Electrochem. Commun. 4 (2002) 384.
[9] V. Hernandez, F.J. Ramirez, T.F. Otero, J.T. Lopez Navarrete, J. Chem. Phys. 100 (1994) 114.
[10] P. Gomez-Romero, Adv. Mater. 13 (2001) 163.

[11] A. Vadivel Murugan, B.B. Kale, C.W. Kwon, G. Campet, A.B. Mandale, S.R. Sainker, C.S. Gopinath, K. Vijayamohanan, J. Phys. Chem. B 108 (2004) 10736.
[12] C.D. Wagner, W.M. Riggs, L.E. Davis, J.F. Moulder, G.E. Muilenberg, Handbook of X-ray Photoelectron Spectroscopy, Perkin-Elmer Corporation, Eden Prairie, MN, 1979.
[13] J.J. Yeh, I. Lindau, At. Data Nucl. Data Tables 32 (1985) 1.
[14] J.M. Cocciantelli, M. Menetrier, C. Delmas, J.P. Doumerc, M. Pouchard, M. Broussely, J. Labat, Solid State Ionics 78 (1995) 143.
[15] H.K. Park, W.H. Smyrl, J. Electrochem. Soc. 141 (1994) L25.
[16] M. Ugaji, M. Hibino, T. Kudo, J. Electrochem. Soc. 142 (1995) 3664.
[17] N.B. Colthup, L.H. Daly, S.E. Wiberley, Introduction to Infrared and Raman Sectropcopy, Academic Press, New York, 1964, p. 276.
[18] J.O. Besenhard, R. Schollhorn, J. Power Sources 1 (1976) 267.
[19] T.A. Kerr, H. Wu, L.F. Nazar, Chem. Mater. 8 (1996) 2005.
[20] A.V. Powell, L. Kosidowski, A. McDowall, J. Mater. Chem. 11 (2001) 1086.